Cellulose (2017) 24:5565–5577
DOI 10.1007/s10570-017-1504-6

ORIGINAL PAPER

Novel modified microcrystalline cellulose-based porous material for fast and effective heavy-metal removal from aqueous solution

Jie Cao · Dongtao Fei · Xiaoling Tian · Yuejun Zhu · Shanshan Wang · Yadong Zhang · Qiangqiang Mao · Mingbo Sun

Received: 5 April 2017 / Accepted: 19 September 2017 / Published online: 13 October 2017

Abstract A novel porous adsorbent with high surface area and rigid structure was prepared by crosslinking oxidized microcrystalline cellulose particles with tetrafluoroterephthalonitrile. N_2 adsorption–desorption measurements revealed the surface area to be 88.32 $m^2\ g^{-1}$ for the porous adsorbent, while it was only 25.74 $m^2\ g^{-1}$ for the sample crosslinked using epichlorohydrin. This porous adsorbent showed excellent performance for fast and efficient removal of low-concentration heavy metals from aqueous solution. Adsorption kinetic study demonstrated that, within 5 min, the removal efficiency for Pb^{2+}, Cu^{2+}, and Cd^{2+} with initial concentration of 10 mg L^{-1} by this adsorbent was 93.2, 87.5, and 72.3 %, respectively. Moreover, the pseudo-second-order model correlated better to the adsorption kinetic data than the pseudo-first-order model. The effects of other factors, e.g., initial solution pH, adsorption temperature, initial metal concentration, and background electrolytes, on the removal efficiency were also analyzed. Additionally, desorption experiments indicated that this adsorbent could be effectively regenerated using dilute HCl solution.

Keywords Microcrystalline cellulose · Heavy-metal removal · Porous materials · Fast adsorption

Introduction

The global problem of micropollutants in water resources has attracted worldwide attention due to the potential harm to human health and the environment. Unlike organic pollutants, heavy-metal ions cannot be degraded by organisms. Consequently, they accumulate in ecosystems and cause gradual toxicity to living organisms (Duan et al. 2013; Fu and Wang 2011). Thus, it is believed that even trace amounts of heavy metals can pose a risk to human beings (Singh et al. 2010; Ma et al. 2015). Various treatment technologies have been established and used for removal of heavy metals from aqueous solution and effluents, including chemical precipitation, ion exchange, oxidation/reduction, membrane processes,

Electronic supplementary material The online version of this article (doi:10.1007/s10570-017-1504-6) contains supplementary material, which is available to authorized users.

J. Cao · Y. Zhu · S. Wang
State Key Laboratory of Offshore Oil Exploitation, Beijing 100028, China

X. Tian
College of Chemical Engineering, China University of Petroleum (East China), Qingdao 266580, China

J. Cao (✉) · D. Fei · Y. Zhang · Q. Mao · M. Sun (✉)
School of Petroleum Engineering, China University of Petroleum (East China), Qingdao 266580, China
e-mail: jcao@upc.edu.cn

M. Sun
e-mail: mbsun@126.com

and electrochemical technologies (Ge et al. 2016; Gollavelli et al. 2013; Xu et al. 2011). However, inherent drawbacks to these methods including incomplete treatment, requirement for large amounts of reagents, high energy consumption, and generation of toxic sludge have hindered their application for heavy-metal removal (Anwar et al. 2009). The adsorption method has been proved to be a suitable process for removal of several kinds of pollutant from aqueous solution owing to its high removal efficiency, low cost, and simple regeneration. Different types of adsorbent materials have been investigated for heavy-metal removal. However, adsorbents have limited application for wastewater treatment because of various drawbacks of such materials, for instance, long time needed to reach equilibrium, unsatisfactory removal efficiency, unsuitability for low-concentration wastewater treatment, etc. (Ji et al. 2012; Ozturk et al. 2004; Wang et al. 2014). Generally, an effective adsorbent should have cellular structure, abundant functional groups, and high mechanical and chemical stability which could endow it with large contact area, adsorption selectivity, and structural stability (Slater and Cooper 2015; Soler-Illia and Azzaroni 2011; Chen et al. 2016). Against this background, microsized porous adsorbents have attracted increasing attention for potential applications in water treatment because their high surface area and highly interconnected porous structure give rise to high transport rates (Tseng et al. 2007).

In recent years, natural and modified biobased materials have drawn public attention due to their environmental friendliness, cost-effectiveness, biodegradability, regenerability, high uptake capacity, and ready availability (Hokkanen et al. 2016; Yi and Zhang 2008; Cao et al. 2017). Various types of cellulose have been tested and shown to exhibit excellent performance for water pollution control (Xu et al. 2013; Kikuchi and Tanaka 2012). Due to the strong hydrogen bond between glucans, microcrystalline cellulose (MCC) has highly crystalline structure. Thus, MCC has unique mechanical and chemical properties, and can be used as a grafted framework to synthesize adsorbents (Liimatainen et al. 2012). However, the adsorption capacity of MCC might not be as excellent as expected without modification due to the lack of strong binding sites for heavy metals (Zhang et al. 2016b). Having three functional hydroxyl groups in its repeating unit, it can be modified by typical alcohol groups, whose oxidation enables introduction of carboxyls. Tetrafluoroterephthalonitrile (TFTPN) is a very important organic intermediate because of its unique properties resulting from fluorine atoms and cyano groups, as well as its rigid structure. Many kinds of high-surface-area and microporous polymers with intrinsic micropores have been prepared using nucleophilic aromatic substitution reaction between hydroxyl groups and TFTPN. Such materials synthesized using TFTPN have been applied in adsorption processes, having potential for application in wastewater treatment (Carta et al. 2009; Budd et al. 2004; Zhang et al. 2016a).

The aim of this work is to develop a cellulose-based material with greater ability for fast and effective removal of low-concentration heavy metals from aqueous solution. As shown in Fig. 1, sequential oxidation of hydroxyl groups on MCC by sodium periodate and sodium chlorite can be applied as a selective reaction route to prepare anionic dicarboxylic cellulose (DCC) (Liimatainen et al. 2012). $NaIO_4$ can oxidize vicinal hydroxyl groups on cellulose molecules to aldehyde groups while simultaneously breaking the carbon–carbon bond of glucopyranose to form 2,3-dialdehyde cellulose (DAC) (Sirviö et al. 2011). Subsequently, $NaClO_2$ selectively oxidizes the aldehyde groups to form chemically stable DCC (Kim and Kuga 2001). We prepared oxidized cellulose crosslinked by TFTPN and epichlorohydrin (EPI), respectively, and investigated the performance of these materials for removal of Cu^{2+}, Pb^{2+}, and Cd^{2+} as model heavy metals. Fourier-transform infrared (FTIR) spectroscopy, N_2 adsorption–desorption isotherm measurements, scanning electron microscopy (SEM), and thermogravimetric analysis (TGA) were conducted to characterize the structure of the adsorbents. The effects of initial solution pH, contact time, initial metal ion concentration, and temperature on their adsorption performance were also investigated. Additionally, we analyzed adsorption kinetics, adsorption isotherms, and adsorption thermodynamics to investigate the metal ion removal mechanism of this novel adsorbent and explored its regeneration experimentally.

Experimental

Materials

Microcrystalline cellulose (MCC) was purchased from Linghu Xinwang Chemical Co. (Huzhou, China).

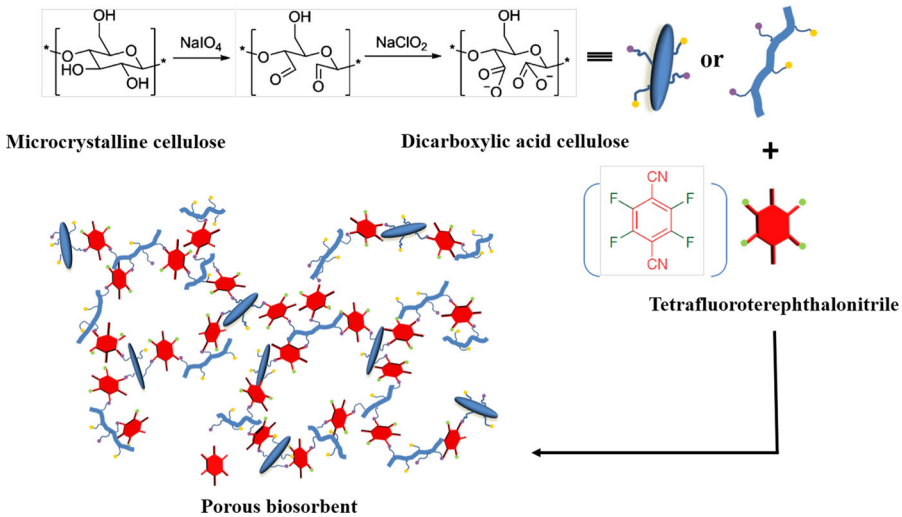

Fig. 1 Preparation of modified microcrystalline cellulose-based porous adsorbent

$NaIO_4$ (99 %), $NaClO_2$ (80 %), acetic acid (99 %), epichlorohydrin (EPI, 99 %), tetrafluoroterephthalonitrile (TFTPN, 99 %), and anhydrous tetrahydrofuran (THF, 99.9 %) were supplied by Shanghai Aladdin Biochemical Technology Co. Ltd. and used without further purification. Other materials were of analytical reagent grade and used as received.

Preparation of adsorbents

Preparation of oxidized cellulose

MCC (1.62 g) was added into 150 mL $NaIO_4$ solution (0.1 mol L^{-1}) and oxidation reaction performed at 50 °C for 4 h in absence of light. The resulting DAC was subsequently filtered, washed, and further reacted with $NaClO_2$ (1.088 g) in 30 mL deionized water, then CH_3COOH (0.26 mL) dissolved in 2 mL H_2O was added dropwise. The reaction was performed for 7 h at room temperature. The oxidized product DCC was filtered and washed with deionized water to remove impurities (Visanko et al. 2015; Varma and Chavan 1994). The particle size distribution of DCC was measured using a Zetasizer (Nano-zs90, Malvern, UK) and is shown in Fig. S1 (Supplementary Information).

Preparation of adsorbents

Porous adsorbents with different ratios of DCC to TFTPN, named S-1 (DCC/TFTPN, 20/1, w/w) and S-2 (DCC/TFTPN, 4/1, w/w), were prepared. A contrast sample, named S-3, was prepared by crosslinking DCC using EPI. The composition of the three samples is presented in Table 1.

The porous adsorbents were prepared using the following steps (Alsbaiee et al. 2016): A dried pressure bottle was charged with DCC, TFTPN, and K_2CO_3 and flooded with N_2 for 5–10 min, then anhydrous THF was added and N_2 was bubbled for 3–5 min. Next, after the N_2 inlet was removed, the bottle was placed in an oil bath (85 °C) and the reactants stirred for 48 h. The resulting brown suspension was cooled and filtered, and remaining K_2CO_3 was removed using HCl (1 mol L^{-1}) until no CO_2 was generated. The recovered brown solid was soaked in H_2O (10 mL) twice for 15 min, THF (10 mL) twice for 30 min, and CH_2Cl_2 (15 mL) once for 15 min. Then, the resulting product was dried in vacuo at 50 °C for 48 h.

The contrast sample was prepared using the following steps: DCC was dissolved in a volume of NaOH solution and vigorously stirred for 15 min at room temperature, then EPI was added dropwise for 150 min at 60 °C. The reactant turned into a yellow gel, which was washed with deionized water then soaked in H_2O (10 mL) twice for 15 min, THF (10 mL) twice for 30 min, and CH_2Cl_2 (15 mL) once for 15 min. The product was obtained after drying in vacuo at 50 °C for 48 h (Udoetok et al. 2016; Anirudhan et al. 2012).

Characterization

Fourier-transform infrared (FTIR) spectroscopic analysis was carried out on KBr pellets of the adsorbents

Table 1 Composition and structural characteristics of the three samples

Sample	DCC (g)	TFTPN (g)	K_2CO_3 (g)	THF (mL)	NaOH (g)	EPI (mL)	H_2O (mL)	Yield (%)	A_{BET} ($m^2\ g^{-1}$)	V_{total} ($cm^3\ g^{-1}$)	D (nm)
S-1	0.2	0.05	0.32	8	–	–	–	82	88.32	0.2860	12.95
S-2	0.2	0.01	0.32	8	–	–	–	74	66.71	0.2281	13.67
S-3	0.2	–	–	–	0.8	2	8	79	25.74	0.1452	22.56

using a Tensor 27 infrared spectrometer (Bruker, Switzerland) over the wavenumber range of 400–4000 cm^{-1}. Thermogravimetric analysis (TGA) of adsorbents was carried out using a thermogravimetric analyzer (Mettler TGA/SDTA851) at heating rate of 10 °C min^{-1} under N_2 flow. After being coated with a thin layer of gold powder, the surface morphology of the adsorbents was analyzed by scanning electron microscopy (SEM) measurements (JSM-7600F, JEOL, Tokyo, Japan). To determine the pore surface area of each sample, N_2 adsorption–desorption measurements were carried out using a specific surface area and pore analyzer (NOVA 3200e, Quantachrome). Before N_2 adsorption measurements, each sample was degassed at 150 °C for 24 h. The specific surface area of each sample was calculated using the Brunauer–Emmett–Teller (BET) equation. Under relative pressure of 0.99, the volume of N_2 adsorbed was measured to calculate the total pore volume of each sample. Desorption isotherms were used to investigate the pore size distribution based on the Barrett–Joyner–Halenda (BJH) method. The average pore size D (nm) for each sample was calculated using Eq. (1) (Lowell et al. 2004):

$$D = 4V_{total}/A_{BET} \tag{1}$$

where V_{total} ($cm^3\ g^{-1}$) is the total pore volume and A_{BET} ($m^2\ g^{-1}$) is the specific surface area.

Adsorption studies

Batch experiments were performed to determine the parameters for adsorption of heavy metals on the adsorbents. In each experimental run, the adsorption behavior was measured by adding 0.050 g adsorbent into 50 mL heavy-metal ion solution. The solution was stirred using a magnetic stirrer throughout the adsorption process. After adsorption, the mixture was separated by centrifugation, and atomic adsorption spectrophotometry (Varian Spectra HP 3510) was used to determine the residual metal concentrations in solution.

To study the effect of pH, the initial pH value was adjusted using 0.1 mol L^{-1} HCL and 0.1 mol L^{-1} NaOH solutions. The adsorption time was varied from 0 to 40 min for kinetic analysis. In each experimental run, 0.05 g of adsorbent was added into 50 mL solution of heavy metals with initial concentration varying from 10 to 85 mg L^{-1} and stirred to obtain the adsorption isotherm. Experiments were conducted at temperatures from 20 to 50 °C for thermodynamic study.

The adsorption capacity q_e and removal efficiency R_e were calculated using Eqs. (2) and (3), respectively:

$$q_e = \frac{(C_0 - C_e) \times V}{m}, \tag{2}$$

$$Re = \frac{(C_0 - C_e)}{C_0} \times 100\,\%, \tag{3}$$

where C_0 (mg L^{-1}) is the initial concentration of heavy metals, C_e (mg L^{-1}) is the concentration of heavy metals at equilibrium, V (L) is the volume of solution, and m (g) is the mass of adsorbent used.

Adsorption kinetic models

Three adsorption kinetic models were used to evaluate the time required to remove heavy metals and determine the rate-controlling mechanism.

The pseudo-first-order kinetic model can be expressed as (Cao et al. 2017)

$$q_t = q_e - q_e e^{-k_1 t}, \tag{4}$$

where q_t and q_e are the adsorption capacity (mg g^{-1}) at time t (min) and at equilibrium, respectively, and k_1 (min^{-1}) is the kinetic rate constant.

The pseudo-second-order kinetic model can be expressed as (Cao et al. 2017)

$$q_t = \frac{k_2 q_e^2 t}{1 + k_2 t q_e}, \quad (5)$$

where k_2 (g mg^{-1} min^{-1}) is the pseudo-second-order rate constant.

The intraparticle diffusion rate model, which determines the rate-controlling step, can be expressed as (Bardajee et al. 2015)

$$q_t = k_3 t^{0.5} + C, \quad (6)$$

where k_3 (mg g^{-1} min$^{0.5}$) is the intraparticle diffusion rate constant and C (mg g^{-1}) is a constant that describes the boundary layer effect.

Adsorption isotherm models

Two common isotherm models were employed to fit the experimental data. The first is the Langmuir isotherm model expressed by Eq. (7) (Cao et al. 2017):

$$q_e = \frac{K_L q_m C_e}{1 + K_L C_e}, \quad (7)$$

where q_e (mg g^{-1}) is the equilibrium adsorption capacity of the adsorbent, C_e is the equilibrium ion concentration in solution (mg L^{-1}), q_m (mg g^{-1}) is the maximum adsorption capacity of the adsorbent, and K_L (L mg^{-1}) is the Langmuir adsorption constant. A dimensionless constant R_L for analysis of the Langmuir isotherm was defined by Eq. (8) (Zhang et al. 2003):

$$R_L = \frac{1}{1 + K_L C_0}. \quad (8)$$

The second adsorption isotherm model is the Freundlich isotherm model, which is expressed as (Cao et al. 2017)

$$q_e = K_F C_e^{1/n}, \quad (9)$$

where q_e and C_e are defined as above, K_F (L mg^{-1}) is the Freundlich constant, and n is the heterogeneity factor.

Adsorption thermodynamics

Based on the Langmuir isotherm, the thermodynamic properties, such as the free energy change (ΔG^0, kJ mol^{-1}), entropy change (ΔS^0, J mol^{-1} K^{-1}), and enthalpy change (ΔH^0, kJ mol^{-1}), are defined as follows (Bardajee et al. 2015):

$$K_L = \frac{q_e}{C_e}, \quad (10)$$

$$\Delta G^0 = -RT \ln(K_L), \quad (11)$$

$$\ln(K_L) = \frac{\Delta S^0}{R} - \frac{\Delta H^0}{RT}, \quad (12)$$

where K_L (L g^{-1}) and q_e (mg g^{-1}) are defined as above, R (8.314 J K^{-1} mol^{-1}) is the universal gas constant, and T (K) is temperature.

Desorption studies

After the 30-min adsorption experiment, the adsorbent was filtered out from the heavy-metal solution. The adsorbed heavy-metal ions were removed from the adsorbent by washing with HCl solution (10 mL, 0.1 mol L^{-1}) for 15 min, then the adsorbent was used again in the same heavy-metal solution. Five consecutive such adsorbent reutilization experiments were performed.

Results and discussion

Characterization of adsorbents

As shown in Fig. 2, the FTIR spectrum of S-1 showed absorbance at 2207 cm^{-1} corresponding to C≡N vibration and absorbance at 1425 cm^{-1} corresponding to C–C aromatic stretching. The band at 1265 cm^{-1} is attributed to C–F stretching vibration (Alsbaiee et al. 2016). Compared with the smaller peak at 1617 cm^{-1} for MCC, the peak at 1630 cm^{-1} for DCC and S-1 can mainly be attributed to adsorption by acetyl group, because the peak strength sharply increased and the wavenumber of this peak also increased after oxidation (Zhou et al. 2013). The FTIR spectra exhibit O–H stretching near 3438 cm^{-1}, C–H stretching vibration at around 2930 cm^{-1}, and intense C–O–C stretching at 1033 cm^{-1}. The FTIR results demonstrate successful introduction of functional groups for adsorption and successful crosslinking of DCC using TFTPN. Due to the weak interaction between hydroxyl group and heavy-metal ions, MCC is not suitable for use as an adsorbent for heavy-metal ion removal. However,

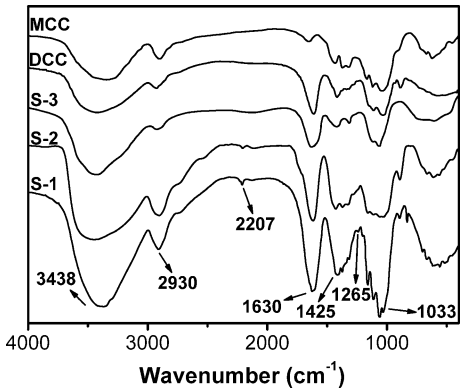

Fig. 2 FTIR analysis of MCC, DCC and the three adsorbents

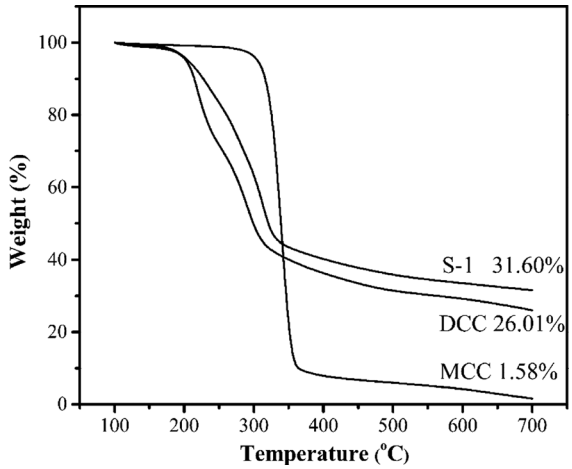

Fig. 3 TGA curves for S-1, DCC, and MCC

there are large amounts of carboxyl groups on the surfaces of S-1, S-2, and S-3, providing adsorption sites for heavy-metal ions. As a result, each sample can be used as an adsorbent.

The thermogravimetric analysis (TGA) and differential thermogravimetric (DTG) curves obtained when the adsorbents were heated from 100 to 700 °C in flowing nitrogen are presented in Fig. 3 and Fig. S2. MCC exhibited obvious weight loss at 340 °C corresponding to the maximum rate of decomposition, with almost complete weight loss at the end (Miranda et al. 2013). The TGA curve for DCC showed significant mass loss at two different temperatures. The first mass loss at temperature lower than 200 °C can be attributed to loss of water, while the second loss at 289 °C can be attributed to decomposition of cellulose component. Adsorbent S-1 demonstrated slight mass loss at 175 and 233 °C and significant mass loss at 312 °C. The peak temperature of its main mass loss is shifted to higher temperature compared with that of DCC, which could be due to the introduction of TFTPN. Thermal degradation of DCC resulted in 26.01 wt% residual mass at 700 °C, compared with 31.60 wt% for S-1, both being much greater than the value of 1.58 wt% for MCC.

As shown in Fig. 4 and Table 1, the differences in the microstructure of the three samples were investigated by BET analysis. For S-1, the BET surface area and pore volume were measured to be 88.32 $m^2\ g^{-1}$ and 0.2860 $cm^3\ g^{-1}$, respectively. However, the BET surface area and pore volume of S-3 were only 25.74 $m^2\ g^{-1}$ and 0.1452 $cm^3\ g^{-1}$, much lower than for S-1. This difference reflects that crosslinking DCC with TFTPN could enhance the surface area and total pore volume more. For similar molecular structures, higher surface area is beneficial for adsorbing heavy metals from wastewater. The porosity of the three samples was further characterized by BJH analysis to determine their pore size distribution. Comparing S-1 and S-3, it was found that S-3 had smaller total pore volume and lower porosity than S-1, and obviously narrower pore size distribution (mainly 3–10 nm). Regarding S-1 and S-2, even using the same crosslinking agent, the curve for S-1 indicated a pore size distribution extending to above pore width of 10 nm. S-1 exhibited a higher cumulative pore size distribution above 3 nm compared with S-2. Thus, this rigid adsorbent crosslinked using TFTPN showed better

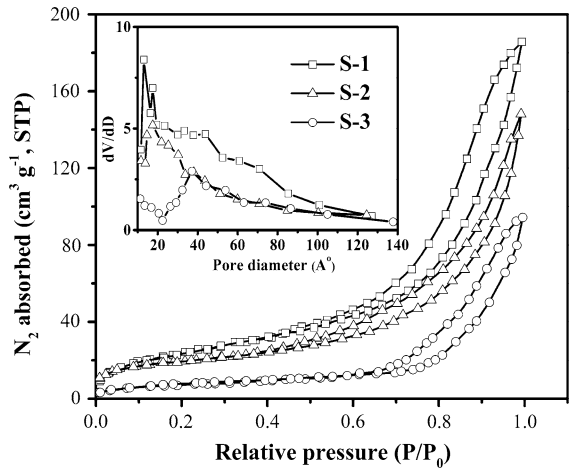

Fig. 4 N_2 adsorption–desorption isotherms and pore size distributions of the three adsorbents

pore structure, and this favorable effect became more pronounced with greater TFTPN addition.

The surface morphology of the three adsorbents was investigated by SEM as shown in Fig. 5. According to the images, S-1 showed many nanopores and small aggregates on its surface (Fig. 5a), which could favor diffusion of metal cations into the adsorbent structure and thus enhance its adsorption capacity. S-3 exhibited an entirely different regular structure, being relatively nonporous. It showed irregular granular structures with dominant size larger than 1 μm (Fig. 5d).

Adsorption studies

Adsorption kinetics

The adsorption kinetic curves (R_e versus t) are illustrated in Fig. 6. It can be seen that the adsorbents exhibited rapid adsorption and that using TFTPN as crosslinking agent obviously improved the removal efficiency. From Fig. 6a, it can be seen that Cu^{2+} was most rapidly removed by S-1, eventually reaching equilibrium in about 5 min, while more than 25 min was required for S-3 to reach equilibrium. The removal efficiency of Cu^{2+} lay in the order S-1 (87.5 %) > S-2 (67.3 %) > S-3 (56.3 %). Figure 6b shows that S-1 exhibited higher adsorption capacity for Pb^{2+} (93.2 %) and Cu^{2+} (87.5 %) than Cd^{2+} (72.3 %). DCC was crosslinked using TFTPN to provide S-1 with high surface area and rigidity. Generally, pores in common adsorbents are twisted and tortuous, resulting in some disadvantages for use as adsorbents, including longer time needed to reach adsorption equilibrium and a more difficult regeneration process caused by the resistance of pore diffusion (Tseng et al. 2007). However, these problems could be mitigated in adsorbent S-1 owing to its special structure and the characteristics of the raw material and crosslinking agent. The produced material had high surface area and rigid structure, promising rapid and efficient removal of low-concentration heavy metals from aqueous solution.

Curve fits for the kinetic models are shown in Figs. S3 and S4. The rate constants, regression coefficients, and other essential parameters for the kinetic rate models are presented in Table 2, revealing that the equilibrium adsorption capacity calculated by fitting the pseudo-second-order kinetic model to the curve was closer to the measured value. The plot of q_t versus $t^{0.5}$ is shown in Fig. S4. Obviously, the plots have nonzero intercept, indicating that intraparticle diffusion occurs throughout the adsorption process (Seifi et al. 2011). Thus, the rate-controlling steps of

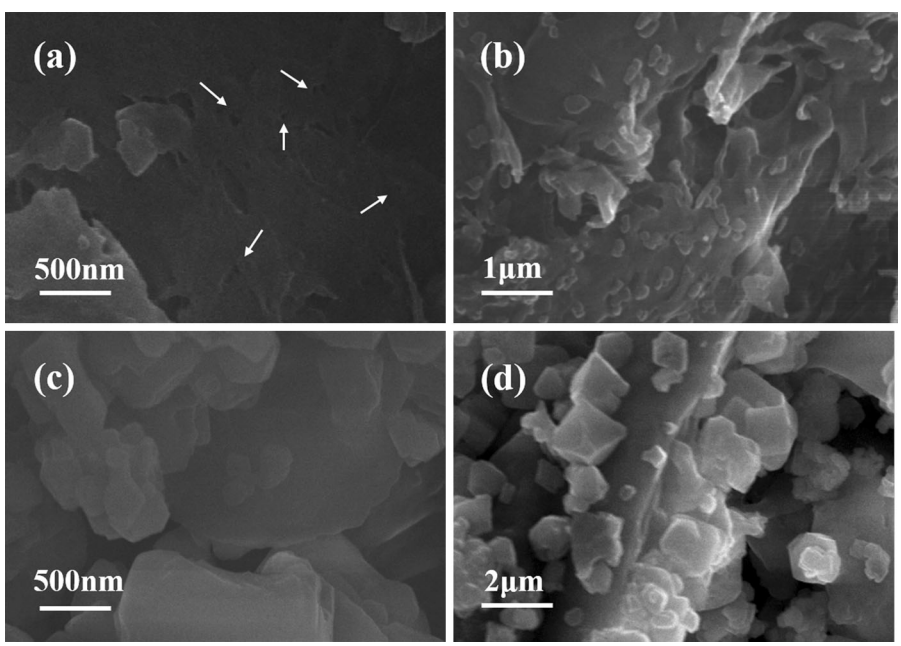

Fig. 5 SEM images of **a**, **b** S-1 and **c**, **d** S-3

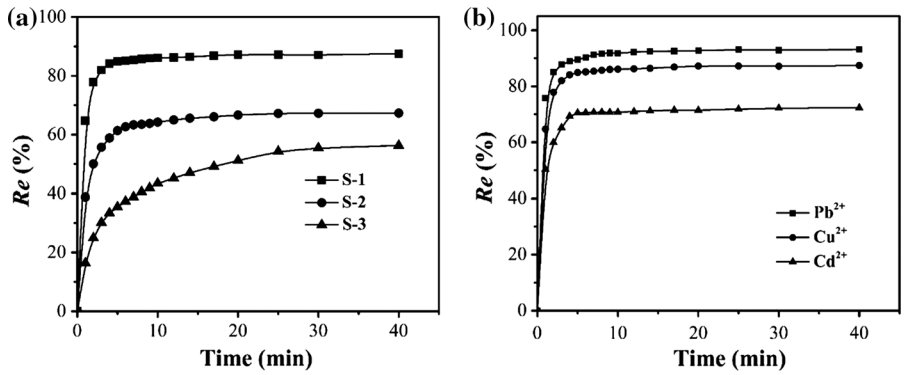

Fig. 6 **a** Kinetic adsorption of Cu^{2+} onto the three adsorbents; **b** kinetic adsorption of Cu^{2+}, Pb^{2+} and Cd^{2+} onto S-1 (conditions: initial metal concentration 10 mg L^{-1}; pH 5.0; 30 °C; adsorbent dose 1 g L^{-1})

the adsorption process include both intraparticle diffusion and liquid film diffusion. There are essentially three stages during adsorption by porous materials: liquid film diffusion (i.e., diffusion to the exterior surface of the adsorbent), intraparticle diffusion, and the equilibrium stage (Mohammed et al. 2015).

Adsorption isotherms

The isotherms for adsorption of heavy metals are shown in Fig. 7, while the calculated parameters of the Freundlich and Langmuir models are summarized in Table 3. The q_e value for each adsorbent increased with increasing concentration until equilibrium was reached. From the results in Table 3, one can see that the adsorption isotherm data matched better with the Langmuir than Freundlich model. The Langmuir model is normally used to describe monolayer adsorption on a homogeneous distribution of sites with a sorption energy that does not consider interaction between adsorbed heavy-metal ions (Guo et al. 2009). Meanwhile, the Freundlich model is suitable for describing multilayer adsorption on a heterogeneous adsorbent surface (Wei et al. 2016; Lin and Juang 2009). According to the results, adsorption occurred on a homogeneous adsorbent surface. It has been reported that a value of n in the range of 2–10 represents good, 1–2 moderate, and < 1 poor adsorption characteristics (Yao et al. 2010). The n values for adsorption of heavy metals onto S-1 indicate that this adsorbent is extraordinarily suitable for heavy-metal adsorption.

Table 2 Pseudo-first-order and pseudo-second-order kinetic parameters for adsorption of heavy metals onto the three adsorbents

Sample	q (mg g^{-1})	Pseudo-first-order model			Pseudo-second-order model		
		R^2	k_1 (min^{-1})	q_e (mg g^{-1})	R^2	$k_2 \times 10^{-3}$ (g mg^{-1} min^{-1})	q_e (mg g^{-1})
S-1							
Pb^{2+}	9.32	0.9940	1.67	9.14	0.9998	46.3	9.39
Cu^{2+}	8.75	0.9964	1.32	8.59	0.9972	34.6	8.90
Cd^{2+}	7.23	0.9927	1.09	7.09	0.9952	31.8	7.39
S-2							
Pb^{2+}	7.87	0.9898	0.89	7.64	0.9968	21.0	8.07
Cu^{2+}	6.73	0.9841	0.76	6.49	0.9988	19.3	6.93
Cd^{2+}	5.99	0.9856	0.61	5.69	0.9924	16.5	6.16
S-3							
Pb^{2+}	6.39	0.9181	0.31	5.74	0.9810	6.65	6.48
Cu^{2+}	5.63	0.9421	0.24	5.14	0.9881	5.26	5.91
Cd^{2+}	4.14	0.9783	0.16	3.72	0.9953	3.95	4.51

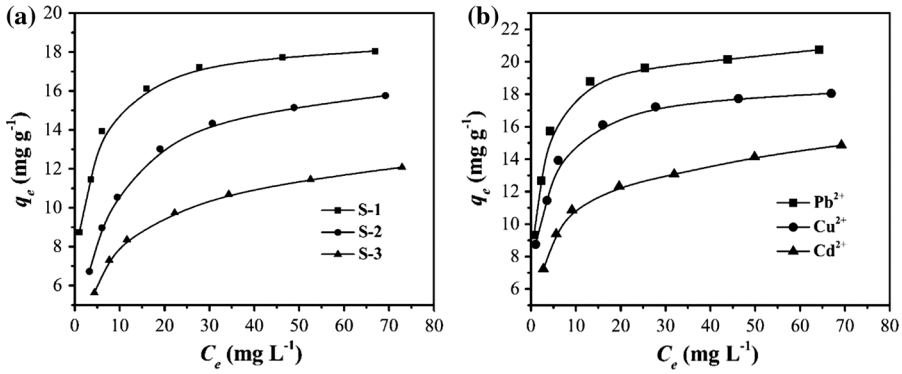

Fig. 7 **a** Equilibrium isotherms for adsorption of Cu^{2+} onto the three adsorbents; **b** equilibrium isotherms for adsorption of Cu^{2+}, Pb^{2+}, and Cd^{2+} onto S-1 (conditions: adsorption time 30 min; pH 5.0; 30 °C; adsorbent dose 1 g L^{-1})

Table 3 Parameters and correlation coefficients for Langmuir and Freundlich adsorption models

	Langmuir model			Freundlich model		
	q_m (mg g^{-1})	K_L (L mg^{-1})	R^2	n	K_F (L mg^{-1})	R^2
S-1						
Pb^{2+}	20.46	0.9161	0.9533	6.560	11.59	0.9051
Cu^{2+}	17.94	0.6808	0.9345	6.282	9.747	0.9267
Cd^{2+}	14.89	0.3081	0.9730	5.111	6.626	0.9594
S-2						
Pb^{2+}	18.02	0.3084	0.9852	4.833	7.702	0.9330
Cu^{2+}	16.78	0.1903	0.9968	4.072	5.862	0.9387
Cd^{2+}	14.00	0.1623	0.9877	3.957	4.646	0.9628
S-3						
Pb^{2+}	13.45	0.3499	0.9520	5.596	6.441	0.9754
Cu^{2+}	12.71	0.1708	0.9885	4.147	4.431	0.9637
Cd^{2+}	11.11	0.1196	0.9937	3.633	3.205	0.9327

The value of R_L can be used to divide adsorption systems into unfavorable ($R_L > 1$), linear ($R_L = 1$), irreversible ($R_L = 0$), and favorable ($0 < R_L < 1$) (Ghorai et al. 2012). As seen in Fig. S6, R_L ranged from 0 to 1, indicating favorable adsorption of heavy metals onto all the adsorbents.

Adsorption thermodynamics

The adsorption thermodynamics was investigated in the temperature range of 293–323 K. The effect of temperature on the adsorption capacity is shown in Fig. 8, revealing a slight decrease in equilibrium adsorption capacity with increasing temperature from 293 to 323 K. The estimated thermodynamic parameters are presented in Table S1 (Supplementary Information). ΔG^0 became more negative as temperature was decreased, indicating a spontaneous nature of the process, being more favorable at low temperature. In addition, its more negative value with decrease of temperature indicates that the adsorption process was promoted by decrease in temperature (Bardajee et al. 2015). The ΔH^0 values were found to lie below zero, indicating exothermic nature of the adsorption process. Negative ΔS^0 indicates decreasing randomness at the solid–liquid interface during the adsorption process, suggesting affinity of the adsorbent for the heavy metals and some structural changes and irreversibility in the adsorption process (Yadav et al. 2013).

Effect of pH

The adsorption capacity for heavy metals was investigated over the pH range of 2.0–6.0. For the three heavy metals, the removal efficiency of the porous adsorbents was greatly affected by the pH value of the

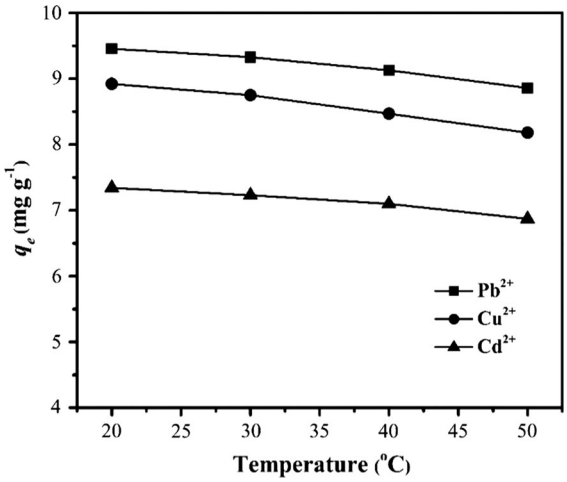

Fig. 8 Effect of temperature on adsorption capacity of S-1 (conditions: adsorption time 30 min; initial metal concentration 10 mg L^{-1}; pH 5.0; adsorbent dose 1 g L^{-1})

solution. As shown in Fig. 9, at low pH, the adsorption capacity of S-1 was insignificant, whereas the removal efficiency increased with increase of the pH value. This is due to alteration of the surface charge on the hydrated heavy metals, because pH affects protonation or deprotonation of surface functional groups (Cao et al. 2017). At low pH, H^+ ions occupy a limited number of possible binding sites on the adsorbent and heavy-metal ions must compete with them for adsorption sites. Increasing the H^+ density restricts the approach of heavy metals to functional groups on the adsorbent because of the repulsive force. With increasing pH, competition from hydrogen ions decreases, more functional groups become negatively charged, and electrostatic repulsion decreases, so adsorption of heavy metals increases (Tseng et al. 2007). In conclusion, adsorption of heavy metals was more favorable at high pH values.

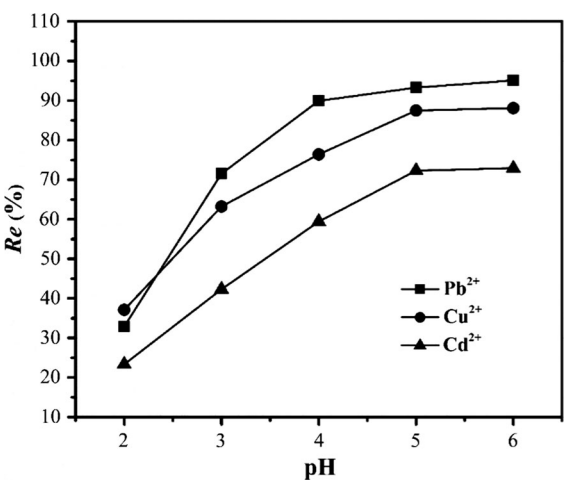

Fig. 9 Effect of initial pH on removal efficiency of S-1 (conditions: adsorption time 30 min; initial metal concentration 10 mg L^{-1}; 30 °C; adsorbent dose 1 g L^{-1})

Effect of background electrolytes

Alkaline and alkaline-earth metal cations, such as Na^+, K^+, and Mg^{2+}, are often present together with heavy-metal cation pollutants in wastewater (Ge et al. 2012). The effects of Na^+, K^+, and Mg^{2+} on the removal efficiency of heavy metals are shown in Fig. S8. Although the removal efficiency for all three heavy-metal ions significantly decreased with increasing background electrolyte concentration in the range of 0–0.08 mol L^{-1}, only slight decrease was observed when the concentration of each background electrolyte was above 0.08 mol L^{-1}. Figure 10 shows the removal efficiency for the three heavy-metal ions when the concentration of background electrolytes was 0.1 mol L^{-1}. One can see that the removal efficiency decreased slightly with increasing concentration of coexisting ions. Mg^{2+} exhibited the most obvious impact on the removal efficiency, while the effects of Na^+ and K^+ ions were negligible. Mg^{2+} shows a greater suppressive effect on adsorption of heavy metals because of the stronger complexation between carboxyl groups and Mg^{2+} ions.

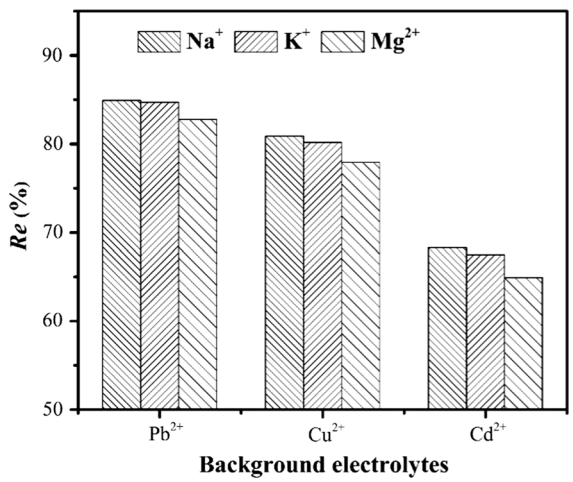

Fig. 10 Effect of background electrolytes on removal efficiency of S-1 (conditions: adsorption time 30 min; initial metal concentration 10 mg L^{-1}; pH 5.0; 30 °C; adsorbent dose 1 g L^{-1}; background electrolyte concentration 0.1 mol L^{-1})

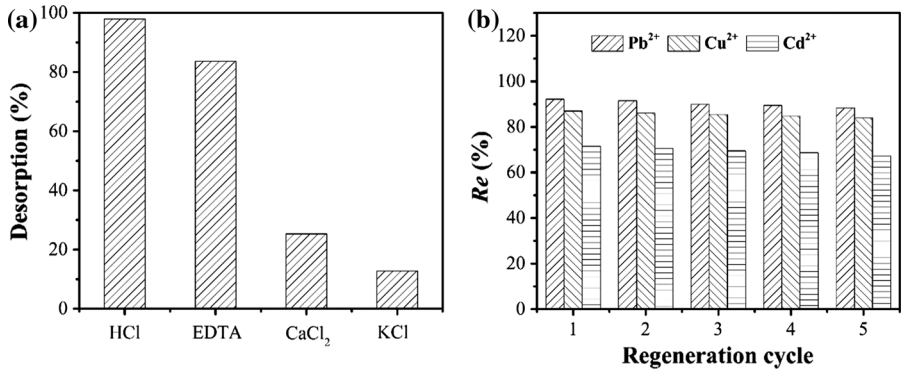

Fig. 11 Regeneration and recycling of S-1: **a** effect of eluting chemical on desorption rate (acid or salt concentration 0.1 mol L^{-1}) and **b** removal efficiency of S-1

Desorption studies

A series of regeneration experiments were performed to investigate the reutilization performance of the adsorbents. HCl, ethylenediaminetetraacetic acid (EDTA), KCl, and $CaCl_2$ were used as eluents for S-1. The results are shown in Fig. 11a. For Cu^{2+} desorption, desorption ratio of 97.9 % was obtained after the adsorbents were treated by HCl (0.1 mol L^{-1}). This indicates almost complete desorption from the loaded adsorbent. However, after being treated by KCl (0.1 mol L^{-1}), the desorption percentage was only 12.7 %. HCl showed the highest desorption ratio for Cu^{2+} and was thus selected for regeneration of S-1. Figure 11b shows the performance of S-1 during the adsorption–desorption cycles. This porous material could be used for several cycles without remarkable changes in performance. The adsorption capacity decreased slightly, which is due to irreversible combination between some active sites on the adsorbent and heavy-metal ions. In addition, according to Fig. 9, the adsorption capability was very weak at low pH, so it is speculated that some carboxyl groups may be protonated during the regeneration process. These results confirm that this porous material could be recycled for adsorption of heavy-metal ions.

Conclusions

We synthesized and characterized a modified microcrystalline cellulose-based porous material. It showed excellent capacity for rapid and efficient removal of low-concentration heavy-metal ions from aqueous solution. Adsorption occurred on the homogeneous surface of the adsorbent with identical binding sites. Thermodynamic analysis revealed that the adsorption process was thermodynamically feasible, spontaneous, and exothermic. Additionally, this adsorbent exhibited good reusability. This novel porous adsorbent is a promising material for wastewater treatment.

Acknowledgments We appreciate financial support from the Open Fund of State Key Laboratory of Offshore Oil Exploitation (CCL2015RCPS0222RNN), National Natural Science Foundation of China (51203187), Fundamental Research Funds for the Central Universities (17CX02053), and Program for Changjiang Scholars and Innovative Research Team in University (IRT_14R58).

References

Alsbaiee A, Smith BJ, Xiao L, Ling Y, Helbling DE, Dichtel WR (2016) Rapid removal of organic micropollutants from water by a porous β-cyclodextrin polymer. Nature 529:190–194

Anirudhan TS, Rauf TA, Rejeena SR (2012) Removal and recovery of phosphate ions from aqueous solutions by amine functionalized epichlorohydrin-grafted cellulose. Desalination 285:277–284

Anwar J, Shafique U, Salman M, Waheed-uz-Zaman AS, Anzano JM (2009) Removal of chromium (III) by using coal as adsorbent. J Hazard Mater 171:797–801

Bardajee GR, Hooshyar Z, Shahidi FE (2015) Synthesis and characterization of a novel Schiff-base/SBA-15 nanoadsorbent for removal of methylene blue from aqueous solutions. Int J Environ Sci Technol 12:1737–1748

Budd PM, Ghanem BS, Makhseed S, Mckeown NB, Msayib KJ, Tattershall CE (2004) Polymers of intrinsic microporosity (PIMs): robust, solution-processable, organic nanoporous materials. Chem Commun 2:230–231

Cao J, Cao H, Zhu Y, Wang S, Qian D, Chen G, Sun M, Huang W (2017) Rapid and effective removal of Cu^{2+} from aqueous solution using novel chitosan and Laponite-based nanocomposite as adsorbent. Polymers 9:5

Carta M, Msayib KJ, Mckeown NB (2009) Novel polymers of intrinsic microporosity (PIMs) derived from 1,1-spirobis(1,2,3,4- tetrahydronaphthalene)-based monomers. Tetrahedron Lett 50:5954–5957

Chen D, Wang L, Ma Y, Yang W (2016) Super-adsorbent material based on functional polymer particles with a multilevel porous structure. NPG Asia Mater 8:e301

Duan C, Zhao N, Yu X, Zhang X, Xu J (2013) Chemically modified kapok fiber for fast adsorption of Pb^{2+}, Cd^{2+}, Cu^{2+} from aqueous solution. Cellulose 20:849–860

Fu F, Wang Q (2011) Removal of heavy metal ions from wastewaters: a review. J Environ Manag 92:407–418

Ge F, Li M, Ye H, Zhao B (2012) Effective removal of heavy metal ions Cd^{2+}, Zn^{2+}, Pb^{2+}, Cu^{2+} from aqueous solution by polymer-modified magnetic nanoparticles. J Hazard Mater 211–212:366–372

Ge H, Huang H, Xu M, Chen Q (2016) Cellulose/poly(ethylene imine) composites as efficient and reusable adsorbents for heavy metal ions. Cellulose 23:2527–2537

Ghorai S, Sinhamahpatra A, Sarkar A, Panda AB, Pal S (2012) Novel biodegradable nanocomposite based on XG-g-PAM/SiO_2: application of an efficient adsorbent for Pb^{2+} ions from aqueous solution. Bioresour Technol 119:181–190

Gollavelli G, Chang C, Ling Y (2013) Facile synthesis of smart magnetic graphene for safe drinking water: heavy metal removal and disinfection control. ACS Sustain Chem Eng 1:462–472

Guo L, Sun C, Li G, Liu C, Ji C (2009) Thermodynamics and kinetics of Zn(II) adsorption on crosslinked starch phosphates. J Hazard Mater 161:510–515

Hokkanen S, Bhatnagar A, Sillanpää M (2016) A review on modification methods to cellulose-based adsorbents to improve adsorption capacity. Water Res 91:156–173

Ji F, Li C, Tang B, Xu J, Lu G, Liu P (2012) Preparation of cellulose acetate/zeolite composite fiber and its adsorption behavior for heavy metal ions in aqueous solution. Chem Eng J 209:325–333

Kikuchi T, Tanaka S (2012) Biological removal and recovery of toxic heavy metals in water environment. Crit Rev Environ Sci Technol 42:1007–1057

Kim UJ, Kuga S (2001) Ion-exchange chromatography by dicarboxyl cellulose gel. J Chromatogr A 919:29–37

Liimatainen H, Visanko M, Sirviö J, Hormi O, Niinimäki J (2012) Enhancement of the nanofibrillation of wood cellulose through sequential periodat-chlorite oxidation. Biomacromolecules 13:1592–1597

Lin S, Juang R (2009) Adsorption of phenol and its derivatives from water using synthetic resins and low-cost natural adsorbents: a review. J Environ Manag 90:1336–1349

Lowell S, Shields JE, Thomas MA, Thommes M (2004) Characterization of porous solids and powders: surface area, pore size and density. Springer, New York

Ma S, Zhan S, Jia Y, Zhou Q (2015) Highly efficient antibacterial and Pb(II) removal effects of $AgCoFe_2O_4$-GO nanocomposite. ACS Appl Mater Interfaces 7:10576–10586

Miranda MIG, Bica CID, Nachtigall SMB, Rehman N, Rosa SML (2013) Kinetical thermal degradation study of maize straw and soybean hull celluloses by simultaneous DSC-TGA and MDSC techniques. Thermochim Acta 565:65–71

Mohammed N, Grishkewich N, Berry RM, Tam KC (2015) Cellulose nanocrystal-alginate hydrogel beads as novel adsorbents for organic dyes in aqueous solutions. Cellulose 22:3725–3738

Ozturk A, Artan T, Ayar A (2004) Biosorption of nickel(II) and copper(II) ions from aqueous solution by Streptomyces coelicolor A3(2). Colloid Surf B Biointerfaces 34:105–111

Seifi L, Torabian A, Kazemian H, Bidhendi GN, Azimi AA, Farhadi F, Nazmara S (2011) Kinetic study of BTEX removal using granulated surfactant-modified natural zeolites nanoparticles. Water Air Soil Pollut 219:443–457

Singh A, Sharma RK, Agrawal M, Marshall FM (2010) Health risk assessment of heavy metals via dietary intake of foodstuffs from the wastewater irrigated site of a dry tropical area of India. Food Chem Toxicol 48:611–619

Sirviö J, Liimatainen H, Niinimäki J, Hormi O (2011) Dialdehyde cellulose microfibers generated from wood pulp by milling-induced periodate oxidation. Carbohydr Polym 86:260–265

Slater AG, Cooper AI (2015) Function-led design of new porous materials. Science 348:988–998

Soler-Illia GJAA, Azzaroni O (2011) Multifunctional hybrids by combining ordered mesoporous materials and macromolecular building blocks. Chem Soc Rev 40:1107–1150

Tseng J, Chang C, Chen Y, Chang C, Chiang P (2007) Synthesis of micro-size magnetic polymer adsorbent and its application for the removal of Cu(II) ion. Colloid Surf A Physicochem Eng Asp 295:209–216

Udoetok IA, Dimmick RM, Wilson LD, Headley JV (2016) Adsorption properties of cross-linked cellulose-epichlorohydrin polymers in aqueous solution. Carbohydr Polym 136:329–340

Varma AJ, Chavan VB (1994) Cellulosic diamines as reaction-incorporated fillers in epoxy composites. Cellulose 1:215–219

Visanko M, Liimatainen H, Sirviö J, Hormi O (2015) A cross-linked 2,3-dicarboxylic acid cellulose nanofibril network: a nanoporous thin-film layer with tailored pore size for composite membranes. Sep Purif Technol 154:44–50

Wang B, Lin H, Guo X, Bai P (2014) Boron removal using chelating resins with pyrocatechol functional groups. Desalination 347:138–143

Wei W, Wang Q, Li A, Yang J, Ma F, Pi S, Wu D (2016) Biosorption of Pb(II) from aqueous solution by extracellular polymeric substances extracted from *Klebsiella* sp. J1: adsorption behavior and mechanism assessment. Sci Rep 6:31575

Xu X, Gao B, Tang X, Yue Q, Zhong Q, Li Q (2011) Characteristics of cellulosic amine-crosslinked copolymer and its sorption properties for Cr(VI) from aqueous solutions. J Hazard Mater 189:420–426

Xu X, Gao B, Tan X, Zhang X, Yue Q, Wang Y, Li Q (2013) Nitrate adsorption by stratified wheat straw resin in lab-scale columns. Chem Eng J 226:1–6

Yadav S, Srivastava V, Banerjee S, Weng C, Sharma YC (2013) Adsorption characteristics of modified sand for the removal of hexavalent chromium ions from aqueous solutions:

kinetic, thermodynamic and equilibrium studies. CATENA 100:120–127

Yao Y, Xu F, Chen M, Xu Z, Zhu Z (2010) Adsorption behavior of methylene blue on carbon nanotubes. Bioresour Technol 101:3040–3046

Yi J, Zhang L (2008) Removal of methylene blue dye from aqueous solution by adsorption onto sodium humate/polyacrylamide/clay hybrid hydrogels. Bioresour Technol 99:2182–2186

Zhang Y, Yang M, Huang X (2003) Arsenic(V) removal with a Ce(IV)-doped iron oxide adsorbent. Chemosphere 51:945–952

Zhang C, Li P, Huang W, Cao B (2016a) Selective adsorption and separation of organic dyes in aqueous solutions by hydrolyzed PIM-1 microfibers. Chem Eng Res Des 109:76–85

Zhang N, Zang G, Shi C, Yu H, Sheng G (2016b) A novel adsorbent TEMPO-mediated oxidized cellulose nanofibrils modified with PEI: preparation, characterization, and application for Cu(II) removal. J Hazard Mater 316:11–18

Zhou Y, Fu S, Zhang L, Zhan H (2013) Superabsorbent nanocomposite hydrogels made of carboxylated cellulose nanofibrils and CMC-g-p(AA-co-AM). Carbohydr Polym 97:429–435